Sl. No.	IIT Ropar List of Recent Publications with Abstract Coverage: June, 2020
1.	A highly efficient bilayer graphene/ZnO/silicon nanowire based heterojunction photodetector with broadband spectral response S Bansal, K Prakash, K Sharma, N Sardana, S Kumar… - Nanotechnology, 2020 **Abstract:** This paper presents three self-powered photodetectors namely, p+-bilayer graphene (BLG)/n+-ZnO nanowires (NWs), p+-BLG/n+-Si NWs/p–-Si and p+-BLG/n+-ZnO NWs/p–-Si. The Silvaco Atlas TCAD software is utilized to characterize the optoelectronic properties of all the devices and is validated by analytical modeling. The proposed dual-junction photodetectors cover broadband spectral response varying from ultraviolet to near-infrared wavelengths. The dual-heterojunction broadband photodetector exhibits photocurrent switching with the rise and fall time of 1.48 and 1.27 ns, respectively. At –0.5 V bias, the highest external quantum efficiency, photocurrent responsivity, specific detectivity and the lowest noise equivalent power of 71%, 0.28 A/W, 4.2×1012 cmHz1/2/W, and 2.59×10–17 W, respectively, are found for the dual-heterojunction device with a wavelength of 480 nm at 300 K. The proposed nanowires based photodetectors offer great potential to be utilized as next-generation optoelectronic devices.
2.	Active Infrared Imaging for Estimation of Sub-Surface Features in a Steel Material K Kaur, R Mulaveesala - Procedia Computer Science, 2020 **Abstract:** Non-destructive Testing (NDT) using infrared thermography plays a crucial role in detecting sub-surface defects in various components/materials. Post-processing of the acquired thermographic data is essential to extract significant information.In this paper, simulated data for infrared thermography of carbon steel has been considered. The steel sample is modeled and simulated with six different defects having different properties. The simulated data is processed with Principal Component Analysis (PCA). Further the thermal data is reconstructed by considering different principal components to ascertain their significance. The reconstructed image sequence from the second principal component provides sub-surface slag defects thermal characteristics with significant Signal to Noise Ratio (SNR) value in comparison with the other principal components.
3.	Activity induced in different rare earth materials using heavy ion oxygen beam; thin layer activation analysis VV Savadi, DP Singh, SK Joshi, I Majeed…PP Singh… - Nuclear Instruments and Methods in Physics Research Section B: Beam Interactions with Materials and Atoms, 2020 **Abstract:** Activities have been measured in spectroscopically pure rare earth materials viz; Terbium, Thulium and Tantalum, based on the remnant radioactivity induced in the material, when bombarded by ^{16}O beam in the energy range from 70 MeV to 110 MeV. The cross sections of a number of isotopes populated through various reaction channels have been measured by the stacked foil activation technique. To measure the activity, yields of the radioactive isotopic products $^{172,171,170}Ta$, $^{171,170}Hf$, ^{171,170,} ^{169}Lu, $^{182,181}Ir$, $^{182,181}Os$, ^{181}Re, $^{194,193,192}Tl$, ^{193,} ^{192}Hg, and $^{192,191,190}Au$ have been determined using the measured cross-sections and subsequently used to measure the activity in these materials which has been found up to 8–16 μm.

4.	Acylation of oxindoles using methyl/phenyl esters via the mixed Claisen condensation–an access to 3-alkylideneoxindoles R Sreedharan, P Rajeshwaran, PKR Panyam…CM Nagaraja… - Organic & Biomolecular Chemistry, 2020 **Abstract:** Predominantly, aggressive acid chlorides and stoichiometric coupling reagents are employed in the acylating process for synthesizing carbonyl tethered heterocycles. Herein, we report simple acyl sources, viz. methyl and phenyl esters, which acylate oxindoles via the mixed Claisen condensation. This straightforward protocol is mediated by LiHMDS and KOtBu and successfully applied to a wide range of substrates. It is a noteworthy transformation that skips the stepwise generation of enolates and acylation, and the reaction is performed at a moderate temperature with no side reactions. This protocol produces the first examples of ortho-substituents in an aryl ring flanked with electron-donating and electron-withdrawing substrates. Interestingly, robust organometallic ferrocenyl methyl ester cleaved under these conditions with ease. Furthermore, biologically important Tenidap's analog was synthesized by this protocol. 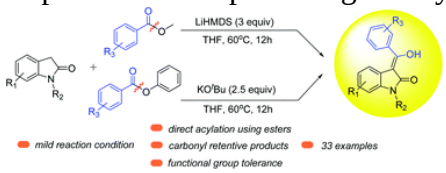
5.	Affordable, Compact and Infection-Free BiPAP Machine GP Singh, N Sardana - Transactions of the Indian National Academy of Engineering, 2020 **Abstract:** Critical cases of COVID-19 require respiratory support provided primarily by mechanical ventilators. But, as per the current trend, about 15% of the cases require hospitalization and less than 5% cases are critical. Due to the massive number of COVID-19 cases all over the world, the ventilator requirement is increasing, and these traditional ventilators are quite expensive and are occupied for the critical cases, thus available in limited numbers. In this regard, BiPAP (Bilevel Positive Airway Pressure) ventilation support can be used for the less critical cases where patients do not require intubation by specialized staff and also minimizing the risk of infection during the procedure. The current article aims to deliver a design of an inexpensive BiPAP with an infection-free exhaust. BiPAP is a mode of ventilation which maintains positive pressure for air intake, and a low or zero pressure is created for expiration. The BiPAP suggested in the current article uses an air blower connected to an Arduino via a speed controller, the level of pressure and breathing rate are programmed in the Arduino, thus, the blower functions in BiPAP mode. The 3D printed mask proposed here comprises of a unique design for the intake and exhalation of air; and comprises of two sizes to fit all adults while avoiding any leakage. The design suggested is further tweaked for emergency use to support up to four patients using a single BiPAP. The mass production of the same would cost approx. INR 6500 or 85 USD.
6.	Assessing the sustainability of a manufacturing process using life cycle assessment technique—a case of an Indian pharmaceutical company RK Sharma, P Sarkar, H Singh - Clean Technologies and Environmental Policy, 2020 **Abstract:** Manufacturing organizations are under continuous pressure to implement sustainability in their activities. There is a need to identify the environmental hotspots in the

	manufacturing processes of the products. In this research life cycle assessment technique has been used to achieve the objective of identifying the maximum impact-generating processes in the production of a pharmaceutical product named 'Paracetamol tablet.' The study identifies the environmental impacts of the paracetamol tablet manufacturing in the endpoint and midpoint impact categories. Three main environmental hotspot processes are identified during this study. The midpoint assessment results show that the 'blister packing' is the top environmental hotspot owing to the consumption of resources of the packaging material. 'Blister packing' has a significant contribution to the seven impact categories. Blister packaging has more than 70% environmental impact in freshwater eutrophication and human toxicity categories. The packaging for the tablet mainly consists of the PVC and aluminum blister, which cause a lot of environmental impact during their production. The 'Blister packing' process is followed by the 'sieving process,' which has more than 80% contribution in land use and metal depletion impact category. To reduce the impacts arising during the 'sieving' process will require improvements in the electricity mix, such as increasing the renewable component in the mix. The third hotspot process is 'steam production,' which shows its presence in almost all the categories varying from 8% to 50%. More efficient ways of steam production like solar-based steam generation will make steam production more environmentally viable. The robustness of the results has been verified using the sensitivity analysis. Possible solutions to reduce the environmental impacts of the hotspot processes have been provided. **Graphical Abstract:** 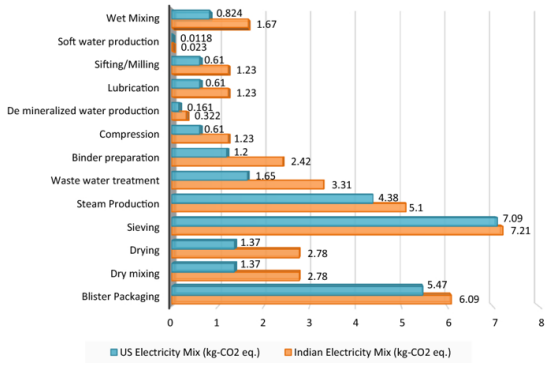
7.	Au0.5Ag0.5 Alloy Nanolayer Deposited on Si-Pyramidal Arrays as Substrates for Surface-Enhanced Raman Spectroscopy Shinki., S Sarkar - ACS Applied Nano Materials, 2020 **Abstract:** Silver (Ag) and gold (Au) are the widely used noble metals for surface-enhanced Raman scattering (SERS) applications in the visible range. However, owing to poor chemical stability of silver and interband transition of gold, thereby hindering the detection process, there has always been a need for an alternate material that can provide intense and stable SERS signals by overcoming the above shortcomings. In this work, we report measurements from a SERS substrate based on a Au–Ag alloy as a SERS-active nanolayer on pyramidal Si (P-Si) array surfaces. Fabrication of the substrate is done by following a simple and cost-effective cosputter deposition method on a prepatterned Si surface produced by a chemical etching process. By suitably integrating the merits of SERS activity of Ag, the chemical stability of Au, and the large field enhancement of P-Si, the alloy Au0.5Ag0.5@P-Si exhibits high SERS sensitivity, homogeneity, reproducibility, and chemical stability far beyond those of the individual elements.

	Using rhodamine 6G (R6G) as a probe molecule, the Au0.5Ag0.5@P-Si substrate shows an ~28 times enhanced SERS signal as compared to that of pure Au@P-Si and ~1.5 times that of pure Ag@P-Si. A detection limit down to 10–9 M concentration of R6G is found in our case. Further, an aging study shows the stability of the SERS signal using the proposed Au0.5Ag0.5@P-Si substrates even after a time span of 30 days. 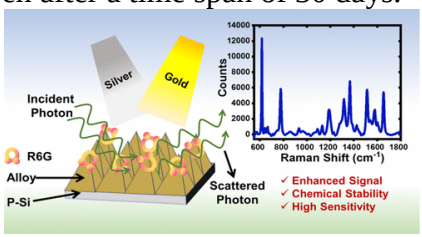
8.	Can India stay immune enough to combat COVID-19 pandemic? An economic query B Rakshit, D Basishtha - Journal of Public Affairs, 2020 **Abstract:** The COVID-19 pandemic has affected different sectors of the economy in an unprecedented way, and this article is an attempt to analyze the economic effect of the outbreak in India. However, before we assess the economic cost associated with the pandemic, we economists fully consider the outbreak as a human tragedy. There has not been any econometric technique that can account the countless human sufferings that the crisis has brought. Through this article, we address several important research questions and demonstrate India's strength to stay immune to combat COVID-19 pandemic. The research questions are as follows. First, what will be the effect of COVID-19 on the Indian economy and how does it affect the different sectors of the economy? Second, how does the pandemic affect the bilateral trade relation between India and China? Third, we question the role of the public health system in dealing with the outbreak of the virus in India. This article also presents the growth projection of the Indian economy by different economic agents. We finally conclude the article by mentioning a few policy recommendations for the Indian economy.
9.	Catalytic Conversion of CO2 to Chemicals and Fuels: The Collective Thermocatalytic/Photocatalytic/Electrocatalytic Approach with Graphitic Carbon Nitride S Samanta, R Srivastava - Materials Advances, 2020 **Abstract:** The rapid industrial development and excessive use of fossil fuels have produced a significantly large volume of CO2 in the atmosphere. The efficient conversion of CO2 to useful chemicals and fuels is an important step towards reducing the concentration of CO2. To overcome the thermodynamic and kinetic barriers involving CO2 activation and conversion, an effective heterogeneous catalyst and a suitable form of energy, such as thermal, photochemical, and electrochemical, are necessary. Considering a wide variety of catalytic materials for CO2 conversion using all forms of energy resources discussed above, earth-abundant carbon materials have exhibited the capability to catalyze the thermal, photo-assisted, and electrochemical mediated conversion of CO2. Among the carbon-based materials, graphitic carbon nitride (g-C3N4) is an inexpensive and sustainable catalyst that can be effectively used for CO2 conversion. Chemical reactivity and optoelectronic properties of g-C3N4 can be finely tailored for its use as a conventional catalyst or photocatalyst or photoelectrocatalyst. This article aims to summarize the synthetic strategies to prepare various types of g-C3N4 materials as conventional catalysts/photocatalysts/photoelectrocatalysts for the improved conversion of CO2 to chemicals

	and fuels. This article reviews the utilization of CO2 as a feedstock for chemicals and fuels synthesis via insertion, carboxylation, and reduction reactions. Further, an in-depth understanding of the catalytic mechanism of various reactions discussed in this article will help in the design of a new generation heterogeneous catalyst for CO2 conversion. A special emphasis is focused on the various parameters influencing the photocatalytic and electrocatalytic CO2 reduction. Finally, the underlying challenges and outlook for the future development of catalysts for CO2 conversion to speciality chemicals and fuels are discussed.
10.	Catalytic-free growth of VACNTs for energy harvesting V Ghai, HS Bedi, J Bhinder, A Chauhan, H Singh, PK Agnihotri - Fullerenes, Nanotubes and Carbon Nanostructures, 2020 **Abstract:** The present study introduces a process to grow micro-honeycomb (μ-HC) vertically aligned carbon nanotubes (VACNTs) using thermal chemical vapor deposition technique. Methane is used as a source of carbon and hydrogen gas as a reducing agent. Where, the fabricated μ-HC structure reported in literature involves complex synthesis process and requires a catalyst layer, the novelty of the process used here lies in the fact that no catalyst layer is used for the growth of CNT network, rather copper foil is used as a substrate. The in-situ cracking of CNTs due to water treatment leads to the formation of μ-HC CNT network, which is confirmed by Raman spectroscopy. Further scanning electron microscopy analysis shows that the length of developed μ-HC CNT is ∼5 μm. Hexagonal μ-HC network shows more than 94% absorption in UV-Vis-NIR wavelength region. The designed process provides high-yield with a low-cost synthesis of vertically aligned CNTs having 3 D microarchitecture. The fabricated CNT network can be used as an electrode for supercapacitor, as an active layer in a photovoltaic cell and most of the energy harvesting devices.
11.	Co-catalyst-free chemical fixation of CO2 into cyclic carbonates by using metal-organic frameworks as efficient heterogeneous catalysts SS Dhankhar, B Ugale, CM Nagaraja - Chemistry–An Asian Journal, 2020 **Abstract:** The concentration of carbon dioxide (CO 2) in the atmosphere is increasing at an alarming rate resulting in undesirable environmental issues. To mitigate this growing concentration of CO 2 , selective carbon capture and storage/sequestration (CCS) are being investigated intensively. However, CCS technology is considered as an expensive and energy-intensive process. In this context, selective carbon capture and utilization (CCU) as a C1 feedstock to synthesize value-added chemicals and fuels is a promising step towards lowering the concentration of the atmospheric CO 2 and also for the production of high-value chemicals. Towards this direction, several strategies have been developed to convert CO 2 , a Greenhouse gas (GHG) into useful chemicals by forming C-N, C-O, C-C, and C-H bonds. Among the various CO 2 functionalization processes known, the cycloaddition of CO 2 to epoxides has gained considerable interest owing to its 100% atom-economic nature producing cyclic carbonates or polycarbonates in high yield and selectivity. Among the various classes of catalysts studied for cycloaddition of CO 2 to cyclic carbonates, porous metal-organic frameworks (MOFs) have gained a special interest due to their modular nature facilitating the introduction of a high density of Lewis acidic (LA) and CO 2 -philic Lewis basic (LB) functionalities. However, most of the MOF-based catalysts reported for cycloaddition of CO 2 to respective cyclic carbonates in high yields require additional co-catalyst, say tetra- n -butylammonium bromide (TBAB). On the contrary, the co-catalyst-free conversion of CO 2 using rationally designed MOFs composed of

	both LA and LB sites is relatively less studied. In this review, we provide a comprehensive account of the research progress in the design of MOF based catalysts for environment-friendly, co-catalyst-free fixation of CO 2 into cyclic carbonates.
12.	Consumer-Brand Engagement With E-Commerce Market Place Brands PK Mohanty, DK Dey - Journal of Electronic Commerce in Organizations (JECO), 2020 **Abstract:** Consumer-brand engagement (CBE) has gained much attention from both the academicians and practitioners. However, despite such scholarly attention, only a few studies have empirically tested the scale of CBE. Moreover, limited attention is paid toward examining the consumer-brand relationships in the e-commerce marketplace context. The study is an empirical investigation of the new ways for examining CBE by testing the impact of consumer advocacy (CA). Furthermore, the study has examined and validated the relationship between consumer involvement (CI) and CBE in the e-commerce marketplace context. The study has further examined the impact of CBE on two outcome variables, viz., positive word-of-mouth (PWOM) and brand usage intention (BUI). A sample size of 408 has been collected randomly from a postgraduate program of a large university located in south India. Various multivariate techniques (Confirmatory Factor Analysis & Path Analysis) have been applied to validate and test the proposed relationships. The results indicate that both CI and CA positively influence CBE. Further, CBE has a positive impact on PWOM and BUI.
13.	Critical-point behaviour of a measurement-based quantum heat engine S Chand, A Biswas - Quantum Information and Measurement, 2019 **Abstract:** Long-range interaction among the particles can substantially enhance the efficiency of a quantum Otto engine, around quantum criticality. We demonstrate this with two trapped ions driven by variable magnetic field, using a measurement-assisted cooling protocol.
14.	Development of HFD-fed/low dose STZ treated female Sprague Dawley rat model to investigate diabetic bone fragility at different organization levels P Sihota, RN Yadav, S Poleboina, V Mehandia…N Kumar - JBMR Plus, 2020 **Abstract:** Type 2 diabetes (T2D) adversely affects the normal functioning, intrinsic material properties and structural integrity of many tissues, and bone fragility is one of them. To simulate human T2D and to investigate diabetic bone fragility, many rodent diabetic models have been developed. Still, the outbred genetically normal non-obese diabetic rat model is not available that can better simulate the disease characteristics of non-obese T2D patients, those have a high prevalence in Asia. In this study, we have used a combination of high-fat diet (4 weeks, 58% kcal as fat) and low dose streptozotocin (STZ, 35 mg/kg, intraperitoneally, at the end of 4th week) treatment to develop T2D in female Sprague Dawley (SD) rats. After eight weeks of the establishment of the T2D model, the femoral bones were excised after sacrificing rats (animal age ~ 21–22 weeks); n = 10 with T2D, n = 10 without diabetes. The bone microstructure (micro-CT), mechanical and material properties (three-point bending, cRPI, nanoindentation), mean mineral crystallite size (XRD), bone composition [mineral-to-matrix ratio, non-enzymatic crosslink ratio (NE-xLR), (FTIR)], and total fluorescent AGE (fAGE) were analyzed. In results, we found that diabetic bone has reduced whole bone strength and compromised structural properties (μCT). The NE-xLR are elevated in the T2D group, and strongly and negatively correlated with post-yield-displacement (PYD), which suggests the possibility of the bone fragility due to lack of glycation control. Along with that the decreased mineral-to-matrix ratio

	and modulus, increased IDI and wider mineral crystallite size in the T2D group evidenced that the diabetic bone composition and material properties have changed, and bone became weaker and tends to easily fracture. Altogether, this model simulates the natural history and metabolic characteristics of late-stage of type 2 diabetes (insulin resistance and as disease progress develops hypoinsulinemia) for non-obese young (and/or adolescent) T2D patients (Asians) and provides potential evidence of the diabetic bone fragility at various organization levels.
15.	Dynamic Sectorization and parallel processing for device-to-device (D2D) resource allocation in 5G and B5G cellular network NMV Mohamad, P Ambastha, S Gautam, R Jain… - Peer-to-Peer Networking and Applications, 2020 **Abstract:** Beyond Fifth Generation (B5G) network aims to provide a very high data rate with minimum latency to an ultra-dense user environment. To achieve this demand, the possible approaches are network-centric and device-centric approach. In a network-centric approach, a new frequency band is introduced, and the existing network infrastructure is modified. The device-centric approach does not require any modification in the existing network infrastructure, and the demand of B5G network is achieved through optimum resource allocation methodology. Device-to-Device (D2D) is an effective device-centric approach that supports the B5G network. In this paper, we propose a dynamic sectorization technique in which eNodeB (eNB) varies the number of sectors dynamically in the network and allocates the Resource Block (RB) to D2D users. Sectoring improves Signal-to-Interference-Noise-Ratio (SINR) and network performance. We derive an expression for the probability of successful transmission and threshold to make a decision on the number of sectors based on available RBs and D2D users in the network. Further, dynamic sectoring helps eNB to perform parallel processing for reducing the denial of the request. Simulation results validate the probability of successful transmission of D2D pairs with available RBs and the effectiveness of parallel processing to reduce the denial of request with improved SINR.
16.	Effect of back reaction on entanglement and subregion volume complexity in strongly coupled plasma C Shankhadeep, P Sanjay, S Karunava - Journal of High Energy Physics, 2020 **Abstract:** The back reaction imparted by a uniform distribution of heavy static fundamental quarks on large Nc strongly coupled gauge theory can be holographically realized as a deformation in AdS blackhole background. The presence of back reaction brings significant changes in to the entanglement structure of the strongly coupled boundary theory at finite temperature. Since the deformed blackhole geometry still remains asymptotically AdS, the gauge/ gravity duality allows us to explore the entanglement structure of back reacted plasma in a quantitative way by computing various measures, e.g holographic en tanglement entropy (HEE) and entanglement wedge cross section (EWCS). We explicitly study the variation of those entanglement measures with respect to the uniform density of heavy static fundamental quarks present in the boundary theory. In particular, we notice enhancement of both HEE and EWCS with respect to quark density. We also study the effect of back reaction on the holographic subregion volume complexity. In this analysis we observe an occurrence of logarithmic divergence proportional to the quark density parameter.

17. [Effect of chain scission on flow characteristics of wormlike micellar solutions past a confined microfluidic cylinder: A numerical analysis]
MB Khan, C Sasmal - Soft Matter, 2020

Abstract: Flow past a microfluidic cylinder confined in a channel is considered as one of the benchmark problems for the analysis of transport phenomena of complex fluids. Earlier experiments show the existence of an elastic instability for the flow of a wormlike micellar solution in this model system after a critical value of the Weissenberg number in the creeping flow regime (G. R. Moss and J. P. Rothstein, J. Non-Newtonian Fluid Mech., 2010, 165, 1505–1515; Y. A. Zhao et al., Soft Matter, 2016, 12, 8666–8681; S. J. Haward et al., Soft Matter, 2019, 15, 1927–1941). This study presents a detailed numerical investigation of this elastic instability in this model system using the two-species VCM (Vasquez–Cook–McKinley) constitutive model for the wormlike micellar solution. Inline with the experimental trends, we also observe the existence of a similar elastic instability in this flow once the Weissenberg number exceeds a critical value. However, we additionally find that the elastic instability in this model geometry is greatly influenced by the breakage and reformation dynamics of the wormlike micelles. In particular, the onset of such an elastic instability is delayed or even may be completely suppressed as the micelles become progressively easier to break. Furthermore, this elastic instability is seen to be associated with the elastic wave phenomena which has been recently observed experimentally for polymer solutions. The present study reveals that the speed of such an elastic wave increases non-linearly with the Weissenberg number similar to that seen in polymer solutions.

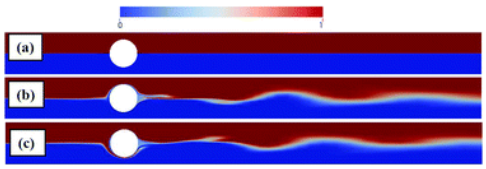

18. [Effect of microstructural features on short fatigue crack growth behaviour in SA508 Grade 3 class I low alloy steel]
R Singh, A Singh, PK Singh, DK Mahajan - International Journal of Pressure Vessels and Piping, 2020

Abstract: Aim of the paper is to understand the effect of microstructural features of SA508 Grade 3 Class I low alloy steel (LAS) on short crack propagation rate under cyclic loading. The complex upper bainitic microstructure of this LAS consists of low angle bainitic ferrite lath boundaries and high angle prior austenite grain boundaries (PAGBs). Compared to bainitic ferrite lath boundaries, the PAGBs provided major hindrance to short fatigue crack propagation in the subject LAS. The high angle PAGBs strongly resist the dislocation motion ahead of the crack tip as the crack tip approaches the PAGBs compared to that of low angle bainitic ferrite lath boundaries. This restriction of dislocation motion ahead of the crack tip based on hindrance provided by PAGBs resulted in retardation in short fatigue crack propagation rate along the crack path. The short fatigue crack propagated at stress intensity factor (SIF) range 'ΔK' values lower than threshold SIF range 'ΔKth' for the long cracks. The growth rate of short fatigue cracks cannot be predicted by Paris law which is applicable for long crack growth. This is due to the fact that crack growth rate undergoes acceleration and retardation in short crack regime because of microstructural effects.

19.	Efficient and Lightweight FPGA-based Hybrid PUFs with Improved Performance NN Anandakumar, MS Hashmi, SK Sanadhya - Microprocessors and Microsystems, 2020 **Abstract:** In recent years, Physically Unclonable Functions (PUFs) have emerged as a promising technique for hardware based security primitives because of its inherent uniqueness and low cost. In this paper, we present an area efficient hybrid PUF design on field-programmable gate array (FPGA). Our approach combines units of conventional RS Latch-based PUF (RS-LPUF) and Arbiter-based PUF (A-PUF) which is then augmented by the programmable delay lines (PDLs) and Temporal Majority Voting (TMV) for performance enhancement. The area of the hybrid PUF is relatively high when compared to few conventional PUF designs, but is significantly small when compared to other composite and hybrid PUF designs reported so far. The measured results on the Xilinx Spartan-6 FPGA demonstrate PUF signatures exhibits good uniqueness, reliability, and uniformity with no occurrence of bit-aliasing.
20.	Electronic Structure Calculations of Reversible Hydrogen Storage in Nanoporous Ti Cluster Frameworks RY Sathe, TJ Dhilip Kumar - ACS Applied Nano Materials, 2020 **Abstract:** Hydrogen is the most potential substitute for fossil fuels in automobiles and shifting to a sustainable energy source. The lack of high-density hydrogen storage materials impedes the use of hydrogen as a fuel. In this study, a porous metal cluster framework (MCF) with Ti cluster as a linker has been reported for the first time. This framework has a pore size of 2.204 nm and a vertical length of 2.597 nm. Using density functional theory, the hydrogen storage capacity and the mechanism of adsorption have been investigated. The Kubas interaction is observed during the hydrogen adsorption process with adsorption energy in the range of 0.22–0.25 eV, and the maximum hydrogen weight percentage is found to be 9.6%. Our findings from Born–Oppenheimer molecular dynamics, van ‘t Hoff desorption study, and occupation number reveal that MCF reversibly adsorbs hydrogen with high gravimetric density under ambient thermodynamic conditions. MCF fulfills the targets of the U.S. Department of Energy, which makes it a promising reversible hydrogen storage candidate. 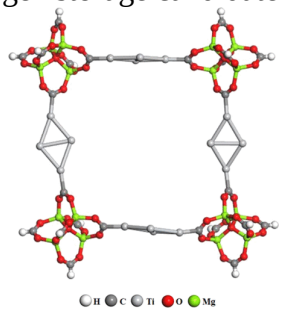
21.	Evidence of narrow range high spin population in incomplete fusion A Sood, P Kumar, RN Sahoo, PP Singh, A Yadav … - Acta Physica Polonica B, 2020 **Abstract:** Particle (p, α)–γ-coincidence experiment has been performed to probe incomplete fusion dynamics in the 12C+169Tm system at 5–7.5 MeV/A. Spin distributions of different reaction products populated via xn and α/2αxn channels have been measured to acquire information about the involved reaction mechanism on the basis of their experimentally observed de-excitation patterns. The spin distributions of direct-α (incomplete fusion) and fusion–

	evaporation (complete fusion) channels are found to be distinct from each other, substantiating their origin in entirely different reaction dynamics. It has been found that CF products span a broad spin range, while ICF products are confined to a narrow spin range localized in the higher spin states. Findings of the present work comprehensively demonstrate that incomplete fusion reactions can be used as a sensitive tool to populate high-spin states in final reaction products, which are not otherwise accessible.
22.	Flow and heat transfer characteristics of a rotating cylinder in a FENE-P type viscoelastic fluid MB Khan, C Sasmal, RP Chhabra - Journal of Non-Newtonian Fluid Mechanics, 2020 **Abstract:** A detailed numerical study on the flow and heat transfer phenomena from a rotating cylinder submerged in a streaming viscoelastic FENE-P fluid has been carried out. The governing equations, along with the FENE-P viscoelastic constitutive equation, have been solved using OpenFOAM over the following ranges of conditions: Reynolds number, $10 \leq Re \leq 100$; Weissenberg number, $0 \leq Wi \leq 10$; non-dimensional rotational velocity or the Rossby number, $0 \leq Ro \leq 2$; polymer extensibility parameter, $10 \leq L2 \leq 500$ and for a fixed value of the Prandtl number of $Pr = 50$. For a stationary cylinder, the separation of the boundary layers is suppressed with the increasing values of the Weissenberg number and the polymer extensibility parameter (L2). Over the range of conditions encompassed in this study, the rotation of the cylinder tends to stabilize the flow for a Newtonian fluid, whereas for a viscoelastic FENE-P fluid, it first induces an inertio-elastic instability which thereby destabilizing the flow with further increase in the rotation rate, viscoelasticity tends to stabilize the flow. The tendency for the onset of this inertio-elastic instability increases with the increasing Weissenberg number, Reynolds number and polymer extensibility parameter. The average Nusselt number increases with the increasing Reynolds number whereas it decreases with the increasing values of the Weissenberg number, polymer extensibility parameter and cylinder rotation rate. On the other hand, the drag coefficient decreases and lift coefficient increases with the cylinder rotation rate irrespective of the fluid type, i.e., Newtonian or viscoelastic. Finally, a simple expression is presented for the average Nusselt number thereby enabling the interpolation of the present results for the intermediate values of the parameters.
23.	Formability Analysis of AA1200 H14 Aluminum Alloy Using Single Point Incremental Forming Process N Kumar, A Singh, A Agrawal - Transactions of the Indian Institute of Metals, 2020 **Abstract:** Single point incremental forming (SPIF) process has the capability to form small/medium-sized part generally used for rapid prototyping applications in automotive and non-automotive industry. Although considerable research has been conducted over the past decades on the formability of various aluminum alloy using SPIF process. This paper presents an investigation on the behavior of AA1200 H14 aluminum alloy by means of SPIF process. The formability of AA1200 H14 in terms of maximum formable wall angle has been evaluated using varying wall angle conical frustum (VWACF) profile. Taguchi method based design of experiment, analysis of variance (ANOVA), signal-to-noise ratio (S/N Ratio) have been employed to identify the significant parameters affecting formability. Utilizing the experimentally acquired results, the S/N ratio (dB) graphs have been drawn and identified the optimal parametric combination for maximizing the wall angle. Further, the formability of the parts has also been evaluated using forming limit curve. The changes in microstructure due to incremental deformation have been studied through scanning electron microscopic analysis.

24.	Generation of uniform-intensity light beams with controllable spatial shapes V Dev, ANK Reddy, V Pal - Optics Communications, 2020 **Abstract:** We present the generation of high-quality light beams of controllable spatial shapes with uniform-intensity distribution based on diffractive optical elements (DOEs) designed by an iterative method that involves spatial Fourier filtering. The Gaussian input beam illuminates the DOEs, and after propagating certain distance transforms into desired uniform-intensity output beams with square, annular, rectangular, hollow square, and plus spatial shapes. We have performed a detailed robustness analysis on the quality of shaped output beams against various types of imperfections in an input beam. It is found that the quality of shaped output beams can be further improved by using additional spatial filtering. Furthermore, we have shown that the quality of shaped output beams remains excellent even when DOE (designed for a specific wavelength) is illuminated by input beam with different wavelengths over a broad range.
25.	Graphene-based tunable multi-band metamaterial polarization-insensitive absorber for terahertz applications P Jain, S Bansal, K Prakash, N Sardana, N Gupta… - Journal of Materials Science: Materials in Electronics, 2020 **Abstract:** This paper presents a graphene-based tunable polarization-insensitive metamaterial absorber (MMA) at terahertz (THz) frequencies. The absorber consists of top patterned gold (Au) layer followed by single layer of graphene, dielectric spacer, and Au layer at bottom. The proposed MMA demonstrates multi-band absorption with the characteristics of both broad- and dual-band absorption by optimizing dimensions (parametric analysis). Broad-band absorption reaches over 90% for the range of 4.57–6.45 THz with the relative absorption bandwidth of 34%, and the absorption peak at 6.86 and 7.20 THz having 98.9 and 95.2% absorption. The normalized impedance and constitutive electromagnetic parameters of the MMA are calculated using the Nicolson–Ross–Weir (NRW) method to validate the absorption rate. Furthermore, proposed absorber is polarization-insensitive upto 90° for transverse electric wave. The tunable characteristic of MMA is achieved by tuning the Fermi energy of graphene with the application of bias voltage. Accordingly, the proposed multi- and broad-band absorbers find its potential applications in spectroscopy detection, imaging, and sensing.
26.	IL@ CQD catalyzed active ester rearrangement for the detection and removal of cyanide ions M Chaudhary, M Verma, P Raj, KC Jena, N Singh - Analyst, 2020 **Abstract:** Carbon Quantum Dots (CQDs) have been extensively employed in various fields of science such as sensing, catalysis, and drug delivery. In this work, ionic liquid coated CQDs (IL@CQDs) have been used as catalysts for the rearrangement of a 1-ethyl-3-(3-dimethylaminopropyl)carbodiimide (EDC) amide coupling intermediate. The rearranged product was confirmed by single crystal structure analysis and it was processed into organic nanoparticles (ONPs). An optical detection method was used to scrutinize the anion sensing properties. The ONPs were found to be sensitive and selective for the recognition of highly toxic cyanide ions through enhancement in the fluorescence intensity. The cyanide ion co-ordinates with the –NH groups of the product and restricts the rotation of molecules around the single bond. The ONPs coated over silica-beads were also showing CN^- recognition in the solid state. The detection limit for CN^- sensing was found to be 3.8 nM, and real sample analysis depicts more than 90% accuracy in detection.

27.	Maximum weight induced matching in some subclasses of bipartite graphs BS Panda, A Pandey, J Chaudhary, P Dane… - Journal of Combinatorial Optimization, 2020 **Abstract:** A subset $M \subseteq EM \subseteq E$ of edges of a graph $G=(V,E)G=(V,E)$ is called a matching in G if no two edges in M share a common vertex. A matching M in G is called an induced matching if G[M], the subgraph of G induced by M, is the same as G[S], the subgraph of G induced by $S=\{v \in V \mid S=\{v \in V \mid v$ is incident on an edge of $M\}M\}$. The MAXIMUM INDUCED MATCHING problem is to find an induced matching of maximum cardinality. Given a graph G and a positive integer k, the INDUCED MATCHING DECISION problem is to decide whether G has an induced matching of cardinality at least k. The MAXIMUM WEIGHT INDUCED MATCHING problem in a weighted graph $G=(V,E)G=(V,E)$ in which the weight of each edge is a positive real number, is to find an induced matching such that the sum of the weights of its edges is maximum. It is known that the INDUCED MATCHING DECISION problem and hence the MAXIMUM WEIGHT INDUCED MATCHING problem is known to be NP-complete for general graphs and bipartite graphs. In this paper, we strengthened this result by showing that the INDUCED MATCHING DECISION problem is NP-complete for star-convex bipartite graphs, comb-convex bipartite graphs, and perfect elimination bipartite graphs, the subclasses of the class of bipartite graphs. On the positive side, we propose polynomial time algorithms for the MAXIMUM WEIGHT INDUCED MATCHING problem for circular-convex bipartite graphs and triad-convex bipartite graphs by making polynomial time reductions from the MAXIMUM WEIGHT INDUCED MATCHING problem in these graph classes to the MAXIMUM WEIGHT INDUCED MATCHING problem in convex bipartite graphs.
28.	Optimization of modulation-assisted drilling of Ti-6Al-4V aerospace alloy via response surface method M Singh, S Dhiman, H Singh, CC Berndt - Materials and Manufacturing Processes, 2020 **Abstract:** The study concerned with optimization of modulation-assisted drilling (MAD) operation for a difficult-to-cut material Ti6Al4 V was carried out via response surface method (RSM). Conventional drilling (CD) has been explored for comparison purposes. Experiments have been designed according to the Central Composite Design (CCD). The impact of machining input parameters on surface roughness (SR), machining power consumption, and tool wear (TW) was investigated for both cases. Pilot experiments were carried out to find out the best modulation range. Further drilling experiments were carried out varying feed rate, spindle speed, and tool diameter. Multiple regression analysis using RSM established relationships between these parameters and responses. ANOVA was used to develop and test the mathematical models. The models were effective in predicting the responses for MAD of Ti6Al4 V. The optimum drilling parameters are a tool diameter (TD) of 2 mm, feed rate (FR) of 0.030 mm/rev and spindle speed (SS) of 2176.87 rpm. SEM and EDS analyzes were performed to investigate the machined surfaces. From the study, it can be concluded that MAD is a promising machining process for difficult-to-cut materials with comparatively less thrust force, surface roughness and tool wear.
29.	Optimization of tumor ablation volume for nanoparticle-mediated thermal therapy D Monga, S Soni, H Tyagi, RA Taylor - International Journal of Thermal Sciences, 2020 **Abstract:** Nanoparticle-assisted thermal therapy for therapeutic tumor specific heating is

	emerging as a promising, minimally-invasive future cancer treatment. For efficient ablation of a tumor with minimum damage to the healthy tissue, the controlling factors must be optimized a-priori. In this study, a two dimensional tissue domain, comprising tumor diameters from 1 cm to 3 cm, were used to optimize the controlling factors of tumor ablation volume. In particular, irradiance, irradiation duration and particle volume fraction were varied to optimize the thermal damage (i.e. calculated from the Arrhenius equation in combination with Pennes' bioheat model). Taguchi's full factorial approach was used with an L27 orthogonal array for the controlling factors. The 'nominal-the-best' approach was implemented to target the optimal ablation volume for each tumor size. The results show that ablation volume increases from irradiance level of 0.75 W/cm2 to 1.50 W/cm2, irradiation duration of 70–80 s to 120–130 s and from a particle volume fraction of 0.00001% to a volume fraction of 0.0001% (i.e. from low to high levels for each parameters) for each tumor size. It was also found that these controlling factors showed the highest gradients for larger tumor diameters. Among the controlling factors, irradiance emerges as the significant factor, with a pronounced effect on tumor ablation volume. Ultimately, the study shows that this approach can be used to define a precise set of controlling factors (specific for each tumor size) to achieve the target ablation volume with minimum variation, resulting in an efficient thermal therapy. **Graphical Abstract:** 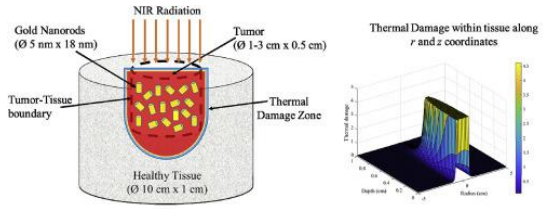
30.	Recognition of Advertisement Emotions with Application to Computational Advertising A Shukla, SS Gullapuram, H Katti… - IEEE Transactions on Affective Computing, 2020 **Abstract:** Advertisements (ads) often contain strong emotions to capture audience attention and convey an effective message. Still, little work has focused on affect recognition (AR) from ads employing audiovisual or user cues. This work (1) compiles an affective video ad dataset which evokes coherent emotions across users; (2) explores the efficacy of content-centric convolutional neural network (CNN) features for ad AR vis-ã-vis handcrafted audio-visual descriptors; (3) examines user-centric ad AR from Electroencephalogram (EEG) signals, and (4) demonstrates how better affect predictions facilitate effective computational advertising via a study involving 18 users. Experiments reveal that (a) CNN features outperform handcrafted audiovisual descriptors for content-centric AR; (b) EEG features encode ad-induced emotions better than contentbased features; (c) Multi-task learning achieves optimal ad AR among a slew of classifiers and (d) Pursuant to (b), EEG features enable optimized ad insertion onto streamed video compared to content-based or manual insertion, maximizing ad recall and viewing experience.
31.	Reinforcing MWCNTs to enhance viscoelastic properties of polyurethane nanocomposites by using nano DMA techniques D Kumar, N Kumar, P Jindal - Journal of Thermoplastic Composite Materials, 2020 **Abstract:** Multi-walled carbon nanotubes (MWCNTs)-reinforced polyurethane (PU) composites

	were fabricated by using solution mixing technique followed by compression molding. Nano dynamic mechanical analysis was carried out to investigate the viscoelastic properties of PU/MWCNTs composites within a frequency range of 5–250 Hz. At higher frequencies (250 Hz), the storage modulus of PU/MWCNTs composites with 10 wt% loading of MWCNTs was enhanced by 148% in equivalence to pristine PU. An improvement of 13.3% in storage modulus was observed at a loading frequency of 250 Hz in comparison to that of a loading frequency of 75 Hz, which indicates that the effect of MWCNTs on storage modulus was more pronounced at higher frequencies. At 75 Hz, a minor composition of MWCNTs (3 wt%) was sufficient to reduce the value of tan δ from 0.20 to 0.15, indicating that the material becomes more elastic after reinforcing MWCNTs. This significant improvement in the mechanical behavior of composite material has been attributed to the uniform dispersion of MWCNTs, and their adhesion with PU molecules. Reported enhancement in the elastic behavior of PU composite will boost the applicability of PU-based composite material for the fabrication of high-strength boots, gloves, and jackets required to absorb high vibration frequencies experienced during conditions such as rock drilling.
32.	Revised lifetime of the 11/2- state in 45Sc via coulomb excitation M Matejska-Minda, PJ Napiorkowski, Kumar R…. A Sood…. - Acta Physica Polonica B, 2020 **Abstract:** A Coulomb-excitation measurement to study low-energy electromagnetic properties of 45Sc has been performed at the IUAC facility in New Delhi, India using a 70 MeV 32S projectile from the 15UD tandem accelerator. The preliminary value of the reduced transition probability B(E2; 11/2 − → 7/2 −) and the resulting lifetime for the 11/2 − state at 1237 keV were determined using the GOSIA code.
33.	Synthesis of Ni (II) Complexes of Novel Naphthalimide Based Heterodipodal Schiff Base Ligands, Structure Characterization and Application for Degradation of Pesticides JS Sidhu, P Raj, T Pandiyan, N Singh - European Journal of Inorganic Chemistry, 2020 **Abstract:** To degrade the highly toxic pesticide into less harmful components, we have synthesized four nickel complexes of naphthalimide based organic ligands. These complexes catalyze the hydrolysis of phosphorothioate bonds of organophosphates in an aqueous medium. The metal complexes ([Ni(L 1) 2] -[Ni(L 4) 2]) were synthesized by the electrochemical method and characterized using single-crystal X-ray crystallography and mass spectrometry. Analytical techniques revealed that complexes are mononuclear and possess octahedral geometry. The rate of degradation of chlorpyriphos and parathion methyl was evaluated using 31 P NMR and LC-MS chromatogram. The byproduct of chlorpyriphos upon catalytic degradation with complex was confirmed from mass spectrometry. It was found that chlorpyriphos degrade into 3,5,6-trichloropyridin-2-ol after 50 minutes of incubation with catalyst. However, parathion methyl took only 20 minutes to hydrolyze into its byproduct. Moreover, the inhibition assay of acetylcholine esterase was performed for pesticides in the presence of metal complex and the interesting outcome was recorded.
34.	Terbium(iii)-coated carbon quantum dots for the detection of clomipramine through aggregation-induced emission from the analyte G Kaur, M Chaudhary, KC Jena, N Singh - New Journal of Chemistry, 2020 **Abstract:** Environmental contamination due to increase in drug levels is reaching an alarming stage. An array of drugs, such as antibiotics, antidepressants, analgesics, and chemotherapy

	drugs, have been found to be polluting agriculture soils and rivers. Here we developed optical sensors based on terbium(III)-coated carbon quantum dots (Tb-CQDs) synthesized by carrying out a single-step one-pot hydrothermal process in an aqueous medium and characterized by using UV-visible, fluorescence, DLS, HRTEM and XRD measurements. Photophysical studies showed the ability of CQD-Tb to act as a chemosensor of the antidepressant drug clomipramine in aqueous medium. A competitive binding assay using CQD-Tb and clomipramine was carried out in the presence of other drugs. No interference resulted from the presence of the other drugs; and hence, the developed chemosensor can be used for selective detection of clomipramine. A functional group analysis was done using FTIR spectroscopy and a mechanism for drug binding with the chemosensor was derived. To target the interfacial behavior with different drugs, vibrational sum-frequency generation (VSFG) spectroscopy was carried out and further confirmed the ability of the synthesized CQD-Tb to act as a chemosensor for the selective detection of clomipramine in the presence of other drugs. 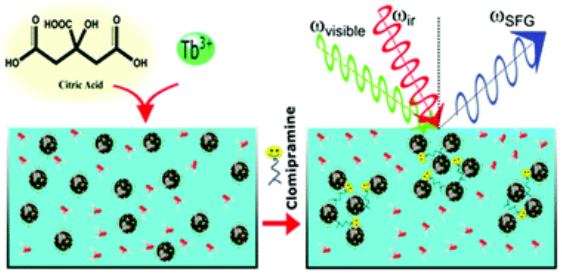
35.	The Role of Cocrystallization-Mediated Altered Crystallographic Properties on the Tabletability of Rivaroxaban and Malonic Acid DP Kale, V Puri, A Kumar, N Kumar, AK Bansal - Pharmaceutics, 2020 **Abstract:** The present work aims to understand the crystallographic basis of the mechanical behavior of rivaroxaban-malonic acid cocrystal (RIV-MAL Co) in comparison to its parent constituents, i.e., rivaroxaban (RIV) and malonic acid (MAL). The mechanical behavior was evaluated at the bulk level by performing “out of die” bulk compaction and at the particle level by nanoindentation. The tabletability order for the three solids was MAL < RIV < RIV-MAL Co. MAL demonstrated “lower” tabletability because of its lower plasticity, despite it having reasonably good bonding strength (BS). The absence of a slip plane and “intermediate” BS contributed to this behavior. The “intermediate” tabletability of RIV was primarily attributed to the differential surface topologies of the slip planes. The presence of a primary slip plane (0 1 1) with flat-layered topology can favor the plastic deformation of RIV, whereas the corrugated topology of secondary slip planes (1 0 2) could adversely affect the plasticity. In addition, the higher elastic recovery of RIV crystal also contributed to its tabletability. The significantly “higher” tabletability of RIV-MAL Co among the three molecular solids was the result of its higher plasticity and BS. Flat-layered topology slip across the (0 0 1) plane, the higher degree of intermolecular interactions, and the larger separation between adjacent crystallographic layers contributed to improved mechanical behavior of RIV-MAL Co. Interestingly, a particle level deformation parameter H/E (i.e., ratio of mechanical hardness H to elastic modulus E) was found to inversely correlate with a bulk level deformation parameter σ0 (i.e., tensile strength at zero porosity). The present study highlighted the role of cocrystal crystallographic properties in improving the tabletability of materials.
36.	Ultrasensitive and Highly Selective Detection of Dopamine by NiFeP based Flexible

	Electrochemical Sensor N Thakur, A Chaturvedi, D Mandal, TC Nagaiah - Chemical Communications, 2020 **Abstract:** A ultrasensitive NiFeP based electrochemical sensor was developed for the selective electrochemical detection of dopamine to address the issue associated with neurological disorders including Parkinson's and Alzheimer's diseases. The novel sensor shows superior selectivity and sensitivity with a lowest detection limit of 0.3 nM and a wide detection range of 10 nM–500 μM and is immune to the interference of ascorbic acid at physiological pH (7.4). A novel flexible sensor was developed with NiFeP coated over Whatman filter paper, which exhibits two liner ranges of 10 nM^{-1} μM and 10 μM–500 μM with an ultra high sensitivity of 756 μA μM^{-1} cm^{-2} and 4.6 μA μM^{-1} cm^{-2} respectively with a wide detection range of 10 nM to 500 μM.
37.	When China sneezes, middle east states get the cold B Rakshit - Journal of Public Affairs, 2020 **Abstract:** The main objective of this study is to extend an economic perspective on the outbreak of COVID-19 pandemic in the Middle East economies. The COVID-19 pandemic, which was initially considered as a Chinese-centric problem, has now affected more than 200 countries worldwide. The impact of the virus on human sufferings is unaccountable. However, economists consider the repercussion of the outbreak as contagious economically as it has been medically. Throughout this paper, we mainly address a few important research questions about the economic aspects of COVID-19. We further highlight three critical channels through which the economic effect of the outbreak can be assessed. Finally, we explain the case of Middle East states and demonstrate the pathways that explain the economic repercussion of this global pandemic on the region. We conclude the paper by providing a few policy recommendations for the Middle East economies to fight the crisis.

Disclaimer: This publication digest may not contain all the papers published. Library has compiled the publication data as per the alerts received from Scopus and Google Scholar for the affiliation “Indian Institute of Technology Ropar” for the month of June 2020. The author(s) are requested to share their missing paper(s) details if any, for the inclusion in the next publication digest.